IEEE Access
Multidisciplinary | Rapid Review | Open Access Journal

SPECIAL SECTION ON EMERGING TECHNOLOGIES FOR ENERGY INTERNET

Received December 20, 2019, accepted January 2, 2020, date of publication January 14, 2020, date of current version February 4, 2020.

Digital Object Identifier 10.1109/ACCESS.2020.2966677

Decoupled Power Control With Indepth Analysis of Single-Phase Electric Springs

QINGSONG WANG[1,2], (Senior Member, IEEE), WUJIAN ZUO[3], MING CHENG[1], (Fellow, IEEE), FUJIN DENG[1], (Member, IEEE), AND GIUSEPPE BUJA[4], (Life Fellow, IEEE)

[1]School of Electrical Engineering, Southeast University, Nanjing 210096, China
[2]Jiangsu Key Laboratory of Smart Grid Technology and Equipment, Zhenjiang 212000, China
[3]State Grid Huzhou Power Supply Company, Huzhou 313000, China
[4]Department of Industrial Engineering, University of Padova, Padua 35131, Italy

Corresponding author: Ming Cheng (mcheng@seu.edu.cn)

This work was supported in part by the Natural Science Foundation of Jiangsu Province under Project BK20170675, and in part by the National Natural Science Foundation of China under Project 51877040.

ABSTRACT Electric spring (ES) as a new effective way to solve the power quality issues caused by the uncertainty of wind and photovoltaic (PV) power, has the advantages of small volume, flexible configuration and low cost. Aiming at improving the dynamic responses of the existing power control for ES-2, a new control with in-depth analysis on the decoupling of the active and reactive powers is proposed in this paper. By introducing second order generalized integrator phase locked loop (SOGI-PLL) and fictitious-axis emulator (FAE) into the control algorithm, the virtual orthogonal voltage and current signals were constructed and the mathematic model of ES-2 in the *dq* axis synchronous rotating reference frame was established. Then, the control system consisting of three closed loops, namely active power loop, current loop and ES voltage loop, is arranged. Among the three loops, a damped proportional resonance (PR) controller is adopted in the ES voltage loop to ensure the accurate control of the output voltage of ES-2. Instead, traditional PI controllers are used for the current and power loops. Finally, the effectiveness of the proposed decoupled power control is validated by both simulation and experimental results.

INDEX TERMS Electric spring, distributed generation, energy storage, microgrid, renewable energy source.

I. INTRODUCTION

As the energy crisis and environmental deterioration in the world are becoming more and more prominent, it is urgent to find new energy to replace the traditional fossil energy. Solar and wind energy, as new and clean renewable energy sources, have been widely used. However, the output power of solar and wind energy is intermittent and unstable, which makes it difficult to predict the power generation. When such new energy is incorporated into the power grid, the uncertainty of output power will affect the power quality and stability of the system which may lead to fault operation of the power system [1].

In order to alleviate such problems, many solutions have been put forward. Currently, the mainstream solutions include reactive power compensation [2], energy storage device [3], direct load control [4] and price incentive [5]. However, these solutions have some limitations. For instance, the equipment for reactive power compensation typically utilizes centralized control so that it may not adapt to the distributed development trend of future power grid. By now, energy storage devices still cost too much, which precludes their massive usage. Direct load control and price incentive use hysteretic control mode, which is not a good choice for localization.

A new compelling way to solve the power quality issues caused by the uncertainty of photovoltaic (PV) and wind power is represented by ES [6]. It creatively applies the concept of mechanical spring to the power system. The basic idea is to classify the loads of a power system into two categories, one is the critical load (CL) that requires higher power quality, such as information center and hospital, the other one is the non-critical load (NCL) that tolerates a certain degree of voltage variation, such as water heater and lighting. By adjusting the magnitude and phase of the output voltage of ES, the active and reactive power absorbed by the ES system

The associate editor coordinating the review of this manuscript and approving it for publication was Huiqing Wen.

is controlled. Specifically, the active power consumed by the NCL is modified while keeping the active power consumed by the CL unaltered in order to improve the power quality for it.

The ES topology has developed for three generations, namely ES-1 [6], ES-2 [7], [8] and ES-3 [9]. In particular, ES-2 replaces the capacitor in the DC side of ES-1 with a voltage source and/or a battery pack, giving ES the capability of regulating both active and reactive power. Compared with the previous two generations, the NCL in ES-3 is not seen visually. The research on ESs is mainly focused on modelling of their dynamics [10], analysis of their application [11], and development of an effective control strategy for them [12]–[16]. In [7], a general study was conducted on the control of ES with active and reactive power compensations at steady state. In [10], the dynamic modelling of ES-1 was formulated, considering only the reactive power compensation. In [11], it is proved that ES can reduce the capacity of energy storage devices in future distributed grid. In [12], Wang et al. proposed the so-called δ control strategy for ES with a proportional resonant (PR) controller for the outer voltage loop and a proportional (P) controller for the inner current loop. In [13], the radial-chordal decomposition (RCD) control was devised, with the radial and chordal components of ES voltage controlling the power angle and voltage amplitude of smart load (SL) respectively. In [14], an input current control scheme is designed for ES focusing on power factor correction. However, it is hard to set the reference of the outer voltage loop. In [15], the collaborative control when power grid with multiple ESs embedded was analyzed. But it's not related to power decoupling. In [16], multifunctional DC electric springs for improving voltage quality of DC grids was discussed.

Space vector control is an effective method for the analysis and design of the active and reactive power decoupling techniques in three-phase grid-tie-inverters. Recently, this method has been extended to single-phase systems [17]. Since only one control variable is available in a single-phase system, a fictitious variable is needed to complete the space vector-based control schemes. To solve this issue, a variety of virtual signal generation algorithms have been proposed [18]–[20]. Unfortunately, these algorithms will introduce additional time delay, which may result in a slower or even oscillatory dynamic response of the control systems. In [21], a fictitious-axis emulator was introduced to prevent the inconvenience above. However, a detailed analysis of how to apply such an algorithm to the power control of ES-2 is still not reported.

Further to the previous discussion, a control strategy setting active power and CL voltage as control objectives is needed for an intensive usage of ES-2 in applications such as households microgrids. Although a simple active and reactive power control was proposed in [22], it is still not satisfactory; for instance, it lacks of a system modelling suitable for the assessment of control parameters. What's more, it is not a complete decoupled power control.

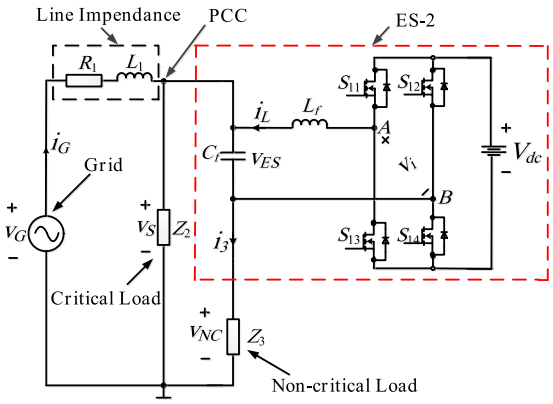

FIGURE 1. Typical application diagram of single-phase ES-2.

Aiming at achieving a decoupled power control with in-depth analysis for ES-2 used in households applications, this paper improves dynamic responses significantly compared with the existing control proposed in [22] by adding an inner current loop and a decoupling network, in which second order generalized integrator (SOGI) algorithm and fictitious-axis emulator (FAE) were introduced to construct the virtual orthogonal voltage and current signals. Besides, space vector method is utilized for the voltage control of the point of common coupling (PCC), selected as the reference vector.

In detail, this paper is organized as follows. Section II reviews the operating principle of ES-2. Section III introduces the novel decoupled power control and explains how it works. Section IV shows the control structure and parameters tuning. Section V presents simulations as well as experiments carried out on an ES-2 operated with the proposed control and discusses the results. At last, Section VI concludes the paper.

II. OPERATING PRINCIPLE OF ES-2

A. ES-2 TOPOLOGY

A typical application diagram of ES-2 is shown in Fig. 1. ES-2 is within the dashed line and contains a bidirectional voltage-source direct-current (DC) power supply, designated as V_{dc}, a single-phase PWM voltage inverter and an LC low-pass filter, represented by the couple L_f and C_f. The fundamental component of the output voltage of the inverter is designated as v_i and its amplitude is instantaneously proportional to V_{dc} as well as to the sinusoidal modulating signal of the PWM inverter.

Such a signal is used to generate the proper gating commands for the switches of the inverter and controls magnitude, frequency and phase of v_i directly. The LC low-pass filter mitigates the high-frequency harmonics at the inverter output voltage. In Fig. 1, R_1 and L_1 denote the impedance of transmission line, Z_2 and Z_3 represent the CL and NCL, v_G is the grid voltage, v_S is the PCC voltage, i_G is the grid current injected into PCC, i_L is current through L_f, i_3 is the NCL current, and v_{ES} is the output voltage of ES-2.

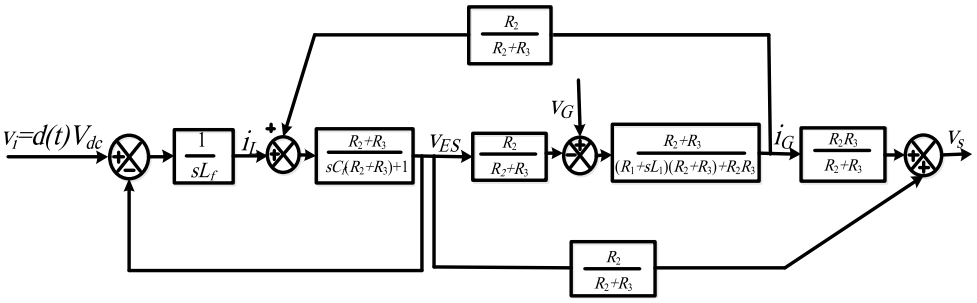

FIGURE 2. The simplified model of ES-2.

B. THE MATHEMATICAL MODEL OF ES-2

Although CL and NCL can be resistive, capacitive or inductive loads, for convenience, CL and NCL are all assumed to be pure resistive in this paper. The state space equations of ES-2 are given as follows.

$$\begin{cases} \dot{x} = Ax + Bu \\ y = Cx \end{cases} \tag{1}$$

where, $x = \begin{bmatrix} i_L \\ v_{ES} \\ i_G \end{bmatrix}$, $u = \begin{bmatrix} v_G \\ v_i \end{bmatrix}$, $y = [v_s]$,

$$A = \begin{bmatrix} 0 & -\frac{1}{L_f} & 0 \\ \frac{1}{C_f} & -\frac{1}{C_f(R_2+R_3)} & \frac{R_2}{C_f(R_2+R_3)} \\ 0 & -\frac{R_2}{L_1(R_2+R_3)} & -\frac{R_1R_2+R_1R_3+R_2R_3}{L_1(R_2+R_3)} \end{bmatrix}$$

$$B = \begin{bmatrix} 0 & \frac{1}{L_f} \\ 0 & 0 \\ \frac{1}{L_1} & 0 \end{bmatrix}, \quad \text{and } C = \begin{bmatrix} 0 & \frac{R_2}{R_2+R_3} & \frac{R_2R_3}{R_2+R_3} \end{bmatrix}.$$

A simple model of ES-2, derived from the above equations, is shown in Fig. 2. The voltage inverter output v_i is denoted with $d(t)V_{dc}$, where $d(t)$ is the modulation signal, under the usual assumptions that i) the inverter switching frequency is much higher than the fundamental frequency, ii) the dynamics of the inverter are negligible, and iii) the LC low-pass filter makes substantially sinusoidal the quantities in the downstream circuit. It is also assumed that the amplitude of the DC voltage source is constant.

III. THE PRINCIPLE OF POWER DECOUPLING CONTROL

A. BASIC THEORY OF POWER CONTROL ON ES-2

DQ rotating frame transformation is commonly used in three-phase system. After the mathematic model of a single-phase ES-2 system is established in a synchronously rotating dq frame, sinusoidal variables of the system can be transformed into DC forms at steady-state. Therefore, even the inverter can be regarded as a special kind of DC converter, thus simplifying the study of the system. In order to implement such transformation, two orthogonal components are required. However, single-phase systems differ from three-phase systems in the fact that they have only one component. Therefore, an extra or virtual orthogonal component is needed to represent the single-phase systems in any coordinate system, whether static or rotating.

For a proper operability of the transformation, the virtual component is set orthogonal to the actual one, i.e. with a phase shift of $-90°$ and with the same magnitude. The existing methods to generate the orthogonal component include the delay 1/4T, the differential method, the SOGI algorithm and so on. In this paper, the SOGI algorithm is adopted in PLL to generate orthogonal voltage signal and acquire phase information of the PCC; FAE is used to construct orthogonal current signal of the ES. For the control of ES, we can assume that i) considering only the fundamental component of the quantities. ii) all the quantities of ES are represented by sinusoidal quantities in slow dynamics or steady state. When the PCC voltage phasor Vs is chosen as the reference vector, the arbitrary sinusoidal voltage and current of PCC are expressed as

$$v_s(t) = \sqrt{2}V_s\cos(\omega t) \tag{2}$$
$$i_G(t) = \sqrt{2}I_G\cos(\omega t + \phi) \tag{3}$$

Meanwhile, the phasor $\boldsymbol{V_s}$ and $\boldsymbol{I_G}$ are:

$$\boldsymbol{V}_s = V_s\angle 0 = V_s \tag{4}$$
$$\boldsymbol{I}_G = I_G\angle\phi = I_G(\cos\phi + j\sin\phi) \tag{5}$$

In $\alpha\beta$ stationary frame, the voltage vector $\boldsymbol{v_{s\alpha\beta}}$ and current vector $\boldsymbol{i_{G\alpha\beta}}$ can be expressed as:

$$\boldsymbol{v_{s\alpha\beta}} = \begin{bmatrix} v_{s\alpha} \\ v_{s\beta} \end{bmatrix} = V_s\begin{bmatrix} \cos(\omega t) \\ \sin(\omega t) \end{bmatrix} \tag{6}$$
$$\boldsymbol{i_{G\alpha\beta}} = \begin{bmatrix} i_{G\alpha} \\ i_{G\beta} \end{bmatrix} = I_G\begin{bmatrix} \cos(\omega t + \phi) \\ \sin(\omega t + \phi) \end{bmatrix} \tag{7}$$

A transformation matrix T that converts a $\alpha\beta$ stationary frame vector to a dq rotating frame vector can be written as

$$\mathrm{T} = \begin{bmatrix} \cos(\omega t) & \sin(\omega t) \\ -\sin(\omega t) & \cos(\omega t) \end{bmatrix} \tag{8}$$

The voltage vector $\boldsymbol{v_{sdq}}$ and current vector $\boldsymbol{i_{Gdq}}$ on rotating frame are shown in (9) and (10).

$$\boldsymbol{v_{sdq}} = \begin{bmatrix} v_{sd} \\ v_{sq} \end{bmatrix} = T \begin{bmatrix} v_{s\alpha} \\ v_{s\beta} \end{bmatrix} = V_s \begin{bmatrix} 1 \\ 0 \end{bmatrix} \tag{9}$$

$$\boldsymbol{i_{Gdq}} = \begin{bmatrix} i_{Gd} \\ i_{Gq} \end{bmatrix} = T \begin{bmatrix} i_{G\alpha} \\ i_{G\beta} \end{bmatrix} = I_G \begin{bmatrix} \cos\phi \\ \sin\phi \end{bmatrix} \tag{10}$$

Thus, the phasor forms of $\boldsymbol{V_s}$ and $\boldsymbol{I_G}$ are expressed as

$$\boldsymbol{V}_s = V_s \angle 0 = V_s = v_{sd} + jv_{sq} \tag{11}$$

$$\boldsymbol{I_G} = I_G \angle \phi = I_G(\cos\phi + j\sin\phi) = i_{Gd} + ji_{Gq} \tag{12}$$

The active power (P) and reactive power (Q) are

$$\begin{aligned} P &= \mathrm{Re}\left(\boldsymbol{V}_s \boldsymbol{I}_G^*\right) = \mathrm{Re}\left(\left\{v_{sd} + jv_{sq}\right\} \cdot \left\{i_{Gd} + ji_{Gq}\right\}\right) \\ &= v_{Sd} i_{Gd} + v_{Sq} i_{Gq} = v_{Sd} i_{Gd} = V_S I_G \cos\phi \end{aligned} \tag{13}$$

$$\begin{aligned} Q &= \mathrm{Im}\left(\boldsymbol{V}_s \boldsymbol{I}_{\boldsymbol{G}}^*\right) = \mathrm{Im}\left(\left\{v_{sd} + jv_{sq}\right\} \cdot \left\{i_{Gd} + ji_{G_q}\right\}\right) \\ &= v_{S_q} i_{Gd} - v_{Sd} i_{G_q} = -v_{Sd} i_{Gq} = V_S I_G \sin\phi \end{aligned} \tag{14}$$

Here, i_{Gd} represents the active current component, and i_{Gq} represents the reactive current component. The PI controllers can be used to control i_{Gd} and i_{Gq} respectively.

B. DQ ROTATING FRAME MODEL OF ES-2

By introducing orthogonal signal generating algorithm to construct corresponding virtual voltage and current signals, the ES-2 application system can be established on a $\alpha\beta$ stationary frame. The equations were given in (15)-(17).

$$\frac{d}{dt}\begin{bmatrix} i_{L\alpha} \\ i_{L\beta} \end{bmatrix} = -\frac{1}{L_f}\begin{bmatrix} v_{ES\alpha} \\ v_{ES\beta} \end{bmatrix} + \frac{1}{L_f}\begin{bmatrix} d_\alpha \\ d_\beta \end{bmatrix} V_{dc} \tag{15}$$

$$\begin{aligned} \frac{d}{dt}\begin{bmatrix} v_{ES\alpha} \\ v_{ES\beta} \end{bmatrix} &= \frac{1}{C_f}\begin{bmatrix} i_{L\alpha} \\ i_{L\beta} \end{bmatrix} - \frac{1}{C_f\,(R_2+R_3)}\begin{bmatrix} v_{ES\alpha} \\ v_{ES\beta} \end{bmatrix} \\ &\quad + \frac{R_2}{C_f\,(R_2+R_3)}\begin{bmatrix} i_{G\alpha} \\ i_{G\beta} \end{bmatrix} \end{aligned} \tag{16}$$

$$\begin{aligned} \frac{d}{dt}\begin{bmatrix} i_{G\alpha} \\ i_{G\beta} \end{bmatrix} &= -\frac{R_2}{L_1(R_2+R_3)}\begin{bmatrix} v_{ES\alpha} \\ v_{ES\beta} \end{bmatrix} \\ &\quad - \frac{R_1R_2 + R_1R_3 + R_2R_3}{L_1(R_2+R_3)}\begin{bmatrix} i_{G\alpha} \\ i_{G\beta} \end{bmatrix} \\ &\quad + \frac{1}{L_1}\begin{bmatrix} v_{G\alpha} \\ v_{G\beta} \end{bmatrix} \end{aligned} \tag{17}$$

Once the $\alpha\beta$ stationary frame model of the system is established, the mathematical model in dq rotating coordinate system can be obtained. The transformation matrix T is multiplied with the expression respectively.

$$\frac{d}{dt}\begin{bmatrix} i_{Ld} \\ i_{Lq} \end{bmatrix} = \begin{bmatrix} 0 & \omega \\ -\omega & 0 \end{bmatrix}\begin{bmatrix} i_{Ld} \\ i_{Lq} \end{bmatrix} - \frac{1}{L_f}\begin{bmatrix} v_{ESd} \\ v_{ESq} \end{bmatrix} + \frac{1}{L_f}\begin{bmatrix} d_d \\ d_q \end{bmatrix} V_{dc} \tag{18}$$

$$\begin{aligned} \frac{d}{dt}\begin{bmatrix} v_{ESd} \\ v_{ESq} \end{bmatrix} &= \begin{bmatrix} 0 & \omega \\ -\omega & 0 \end{bmatrix}\begin{bmatrix} v_{ESd} \\ v_{ESq} \end{bmatrix} + \frac{1}{C_f}\begin{bmatrix} i_{Ld} \\ i_{Lq} \end{bmatrix} - \frac{1}{C_f(R_2+R_3)} \\ &\quad \times \begin{bmatrix} v_{ESd} \\ v_{ESq} \end{bmatrix} + \frac{R_2}{C_f(R_2+R_3)}\begin{bmatrix} i_{Gd} \\ i_{Gq} \end{bmatrix} \end{aligned} \tag{19}$$

$$\begin{aligned} \frac{d}{dt}\begin{bmatrix} i_{Gd} \\ i_{Gq} \end{bmatrix} &= \begin{bmatrix} 0 & \omega \\ -\omega & 0 \end{bmatrix}\begin{bmatrix} i_{Gd} \\ i_{Gq} \end{bmatrix} - \frac{R_2}{L_1\,(R_2+R_3)}\begin{bmatrix} v_{ESd} \\ v_{ESq} \end{bmatrix} \\ &\quad - \frac{R_1R_2 + R_1R_3 + R_2R_3}{L_1\,(R_2+R_3)}\begin{bmatrix} i_{Gd} \\ i_{Gq} \end{bmatrix} + \frac{1}{L_1}\begin{bmatrix} v_{Gd} \\ v_{Gq} \end{bmatrix} \end{aligned} \tag{20}$$

It is shown in (20) that there is a coupling relationship between i_{Gd} and i_{Gq}. As a result, the feedforward decoupling process can be introduced to realize the current decoupling, which can be seen from the last items in (21) and (22).

$$\begin{aligned} v_{ESd} &= -\left(K_p + \frac{K_i}{s}\right)\left(i_{Gd}^* - i_{Gd}\right) \\ &\quad + \frac{R_2+R_3}{R_2}\omega L_f i_{Gq} + \frac{R_2+R_3}{R_2}v_{Gd} \end{aligned} \tag{21}$$

$$\begin{aligned} v_{ESq} &= -\left(K_p + \frac{K_i}{s}\right)\left(i_{Gq}^* - i_{Gq}\right) \\ &\quad - \frac{R_2+R_3}{R_2}\omega L_f i_{Gd} + \frac{R_2+R_3}{R_2}v_{Gq} \end{aligned} \tag{22}$$

It should be remarked that (21) and (22) are related to ES voltage instead of the output of the inverter. Among them, $i_{Gd}*$ and $i_{Gq}*$ are the given values of d axis current i_{Gd} and q axis current i_{Gq}, K_p is the proportional gain of PI controller and K_i is the integral term gain.

Substituting (21) and (22) into (20) yields

$$\begin{aligned} L\frac{d}{dt}\begin{bmatrix} i_{Gd} \\ i_{Gq} \end{bmatrix} &= -\left[\frac{R_1R_2 + R_1R_3 + R_2R_3}{(R_2+R_3)} + \left(K_p' + \frac{K_i'}{s}\right)\right] \\ &\quad \times \begin{bmatrix} i_{Gd} \\ i_{G_q} \end{bmatrix} + \left(K_p' + \frac{K_i'}{s}\right)\begin{bmatrix} i_{Gd}^* \\ i_{G_q}^* \end{bmatrix} \end{aligned} \tag{23}$$

The feedforward decoupling algorithm is revealed by (23) based on (21) and (22), which realizes the decoupling control of the current inner loop.

IV. THE CONTROL STRUCTURE AND PARAMETERS TUNING OF POWER DECOUPLING CONTROL

A. CONTROLLER STRUCTURE OF ES VOLTAGE

According to the above analysis, when PCC voltage is used as reference vector, the power injected at PCC point will be directly related to i_{Gd} and i_{Gq}. In order to achieve precise control of injected active power and reactive power, a power outer loop can be built outside the current loop. However, it must be pointed out that the above decoupling method is based on the output voltage of ES-2 designated as v_{ES} instead of the output of the inverter designated as v_i which is actually controlled by PWM. Therefore, an additional inner controller must be added to control the output voltage of ES-2 be consistent with the output of the current controller.

A simple model of ES-2 has been shown in Fig. 2. However, it is not the best model for analysis and design the v_{ES} controller, because of the existence of coupling term $R_2/(R_2+R_3)$ between v_{ES} and i_G. According to the classical control theory, branch point can be relocated from i_G to v_{ES}, which is shown in Fig. 3(a). Furthermore, $G_1(s)$ can be regarded as a negative feedback term. They can be put together, shown in Fig. 3(b).

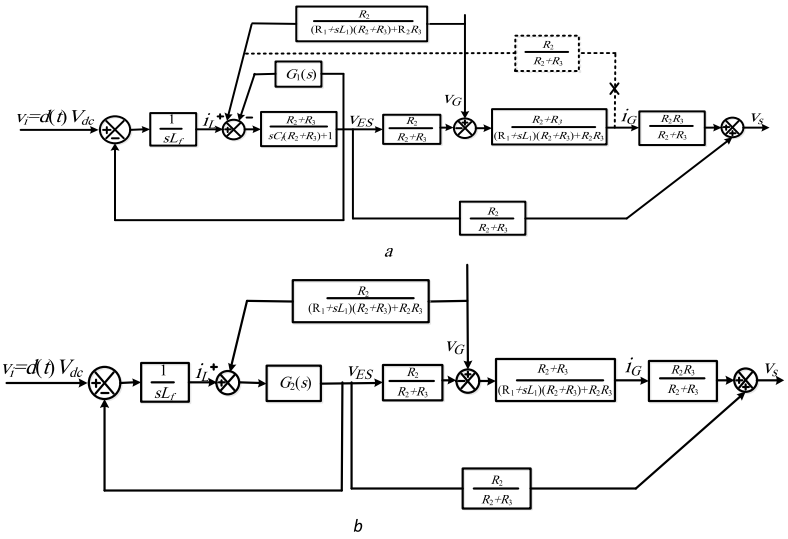

FIGURE 3. The simplified model of ES-2. a Relocation of branch point of input current *i* b Equivalent circuit of (a).

Where,

$$G_1(s) = \frac{R_2^2}{((R_1 + sL_1)(R_2 + R_3) + R_2R_3)(R_2 + R_3)} \tag{24}$$

$$G_2(s) = \frac{(R_1+sL_1)(R_2+R_3)+R_2R_3}{sCf((R_1+sL_1)(R_2+R_3)+R_2R_3)+R_1+sL_1+R_2} = \frac{Z_0}{sCfZ_0+1}$$

$$Z_0 = \frac{(R_1 + sL_1)(R_2 + R_3) + R_2R_3}{(R_1 + sL_1) + R_2} \tag{25}$$

Now, the system can be seen as two independent subsystem series with each other. The effectiveness of the disturbance of the v_G on v_{ES} can be equivalent to a current disturbance i_{dis}.

Active damping was commonly used to damp transient oscillations on the output LC filter. A virtual resistor is used to simulate the roles of a resistor in the output LC filters. Due to the virtual resistor, the oscillation can be damped effectively without sacrificing the power efficiency. Here, the feedback of capacitor's current [23] was adopted. The effectiveness of coefficient was shown in Fig. 4. With the increasing of the coefficient, the better behavior it is. In order to achieve almost zero error at steady state in sinusoidal tracking and disturbance rejection, an approximating non-ideal proportional resonant (PR) controller is adopted.

The expression of the non-ideal PR controller is given as follows.

$$G_{C1}(s) = K_p + \frac{2K_i\omega_c s}{s^2 + 2\omega_c s + \omega_0^2} \tag{26}$$

where, K_p and K_i are gain constants, ω_0 is grid frequency (314 rad/s) and ω_c is cut-off frequency.

The control structure of v_{ES} is shown in Fig. 5(a), where $G_{C1}(s)$ is the controller; the red dashed box is the active damping term; H_1 is feedback coefficient of the capacitor's current; K_{pwm} is the gain of the inverter. Furthermore, the feedback of the v_{ES} can be relocated in the disturbance point.

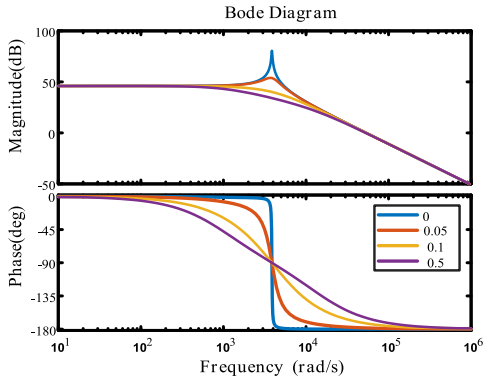

FIGURE 4. The bode diagrams of the system with different damping coefficients.

It must be pointed out that the sampling time and calculating time (about $1.5T_S$ delay) was ignored because of the enough high sampling frequency. The final structure of control loop is shown in Fig. 5(b), where

$$G_3(s) = \frac{sZ_0L_f}{L_fC_fZ_0s^2 + s\left(L_f + sZ_0H_1C_fK_{pwm}\right) + Z_0} \tag{27}$$

The effectiveness of K_p, K_i and ω_c on the controller's performance has already been well reported in [24].

In short, K_i has little influence on the bandwidth but the gain of the controller increases while K_i increases. The bandwidth can be widened by tuning ω_c appropriately. Meanwhile, the magnitude and the phase increase when ω_c increases. With K_p increases, the magnitude of the PR controller increases, but the phase magnitude decreases. Based on the theory analysis, the PR controller gains are chosen as $K_p = 0.2$, $K_i = 10$ and $\omega_c = 5$ in this paper. The parameters of the main circuit of the ES application system are shown in Table 1. The open loop Bode diagram is shown in Fig. 5(c). The bandwidth of closed loop is about 2.6kHz. According to (21) and (22), the references of the current loop are V_{esdref}

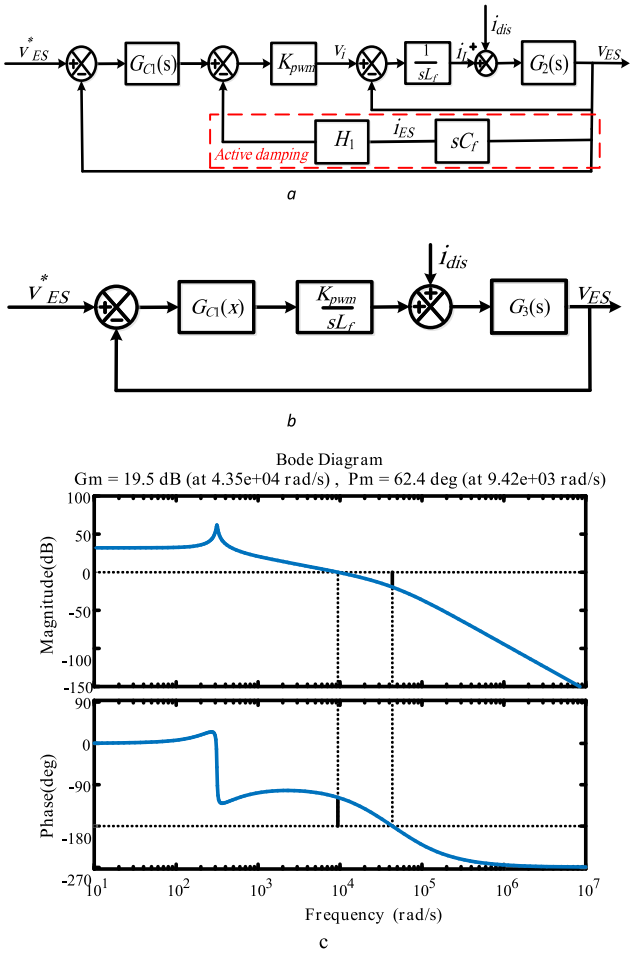

FIGURE 5. Design of control loop of ES voltage. a The control structure of ES voltage b The simplified control loop of (a) c Bode diagram of open loop transfer function of (b).

TABLE 1. Parameters for simulations and experiments.

Items	Values
PCC voltage (V_S)	110V
DC bus voltage (V_{dc})	200V
line resistance (R_1)	1.64Ω
line inductance (L_1)	30.4mH
critical load (Z_2)	1603.4Ω
non-critical load (Z_3)	51.05Ω
inductance of ES filter (L_f)	2.3mH
capacitance of ES filter (C_f)	26μF
Switching frequency	10kHz

and V_{esqref}, respectively. Thus, an additional ES voltage loop is used to keep i_d and i_q independent.

B. CURRENT CONTROL STRUCTURE OF ES-2

The structure using the vector control of a current regulated ES-2 is depicted in Fig. 6(a).

It must be pointed out that the cross-decoupling term and voltage feedforward term were ignored in the structure to

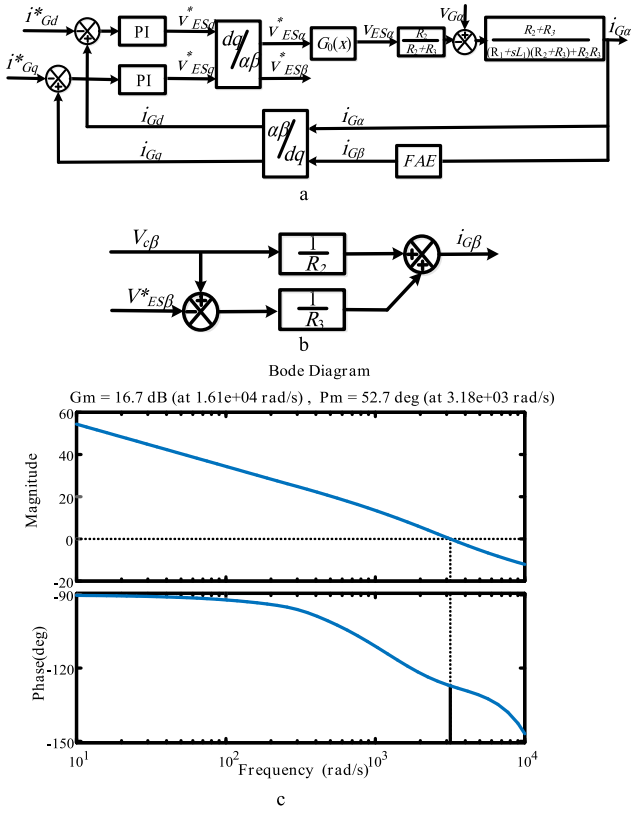

FIGURE 6. Design of current loops. a General structure using vector control b Structure of FAE [25] c Open loop bode diagram.

simplify the analysis. The d axis is aligned with the PCC voltage, while the q axis is orthogonal to it. The dq frame current references i^*_{Gd} and i^*_{Gq} are related to active and reactive power, respectively. The measured current i_G is the feedback signal for the current controller. An additional orthogonal current $i_{G\beta}$ is generated by fictive-axis emulator.

The detailed structure diagram of fictive-axis emulator is shown in Fig. 6(b). In which, SOGI PLL is used to detect the PCC voltage and construct $V_{c\beta}$. $V^*_{ES\beta}$ is the predefined value of β axis. $G_0(s)$ is the closed loop transfer function of ES voltage loop.

Under the cutoff frequency of ES voltage loop, the closed loop transfer function can be assumed to be 1. Thus, the open loop transfer function of current regulator can be expressed as

$$G_C(s) = \left(K_p + \frac{K_i}{s}\right)\left(\frac{R_2}{(R_1+L_1 s)(R_2+R_3)+R_2R_3}\right) \quad (28)$$

Now it remains to determine the parameters of PI controllers. There are many methods and criteria for PI controller synthesis. In this paper, the cutoff frequency f_c and the phase margin are used as the design objectives.

$$\left(K_p + \frac{K_i}{s}\right)\left(\frac{R_2}{(R_1+L_1 s)(R_2+R_3)+R_2R_3}\right)\Bigg|_{s=j\omega_c} = 1\angle\varphi_m - \pi \quad (29)$$

The bandwidth and phase margin are set to 1kHz and 65° to achieve rapid and smooth response. The parameters

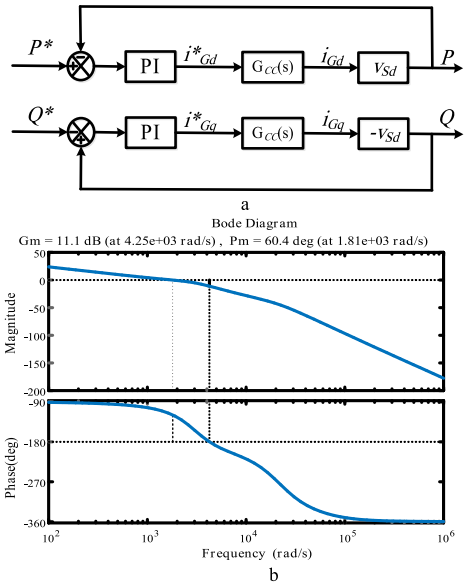

FIGURE 7. The structure and open loop Bode diagram of power control loop a The structure of the power control loop b Open loop bode diagram of power control loop.

of the controller could be estimated by solving (28). In this paper, $K_p = 60$; $K_i = 2.5e5$, and the final open loop Bode diagram of current loop is shown in Fig. 6(c).

C. POWER CONTROL STRUCTURE OF ES-2

The function of the power loop is to confirm the power accuracy tracking. The structure of the power loop was shown in Fig. 7(a). The open loop transfer function was given in (29), where $G_{CC}(s)$ is the closed loop transfer function of the current loop, shown as follows.

$$G(s) = v_{Sd}\left(K_{pv} + \frac{K_{iv}}{s}\right) G_{CC}(s) \tag{30}$$

$$G_{CC}(s) = \frac{G_C(s)}{1 + G_C(s)} \tag{31}$$

The cutoff frequency f_c and the phase margin can also be used as the design objectives to determine the parameters of the controller. The bandwidth of power loop should be lower than the current loop to ensure the performance of the current control. Here the bandwidth and phase margin are set to 300Hz and 60° to achieve rapid and smooth response. The parameters of the controller could be estimated similar to the current controller. Here, $K_{pv} = 0.0001$; $K_{iv} = 10$. Considering the current loop and the ES voltage loop, the open loop Bode diagram is shown in Fig. 7(b).

V. SIMULATIONS AND EXPERIMENTS

To check the effectiveness of the proposed control, a feasibility study has been carried out in the laboratory, by coupling the ES-2 to an application as depicted in Fig. 8.

In Fig. 8(a), v_G is obtained from the grid through a transformer. Z_1 emulates the line impedance between PCC and v_G. Z_2 is connected to PCC directly. In this part, three closed

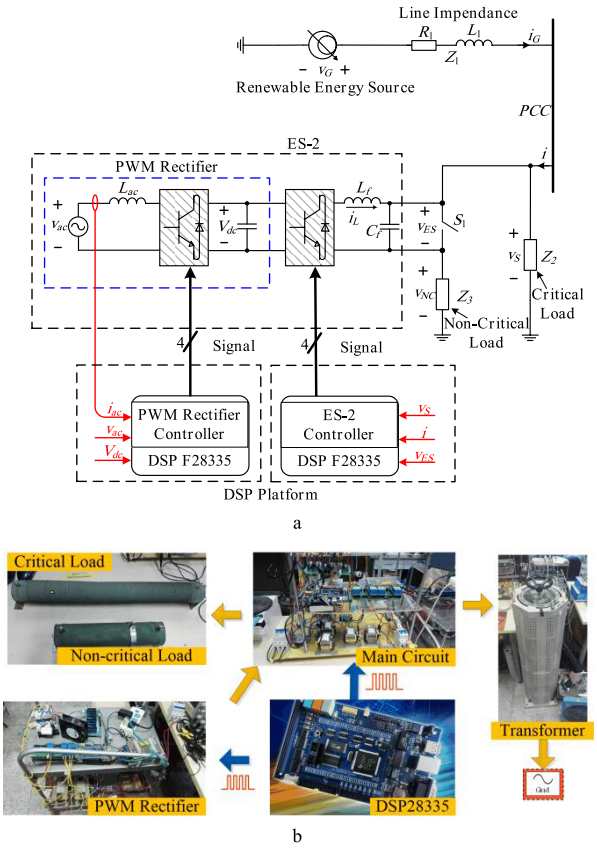

FIGURE 8. Application and setup of experiments. a Diagram of implementation b Picture of experimental setup.

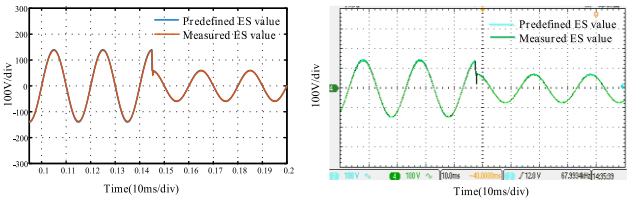

FIGURE 9. Simulation and experiment waveforms of ES voltage loop when predefined magnitude value of ES voltage steps from 120V to 60V.

loops will be validated separately through simulations and experiments.

From Fig. 9 to Fig. 11, the subfigures on the left are the simulation waveforms while experiment waveforms are on the right. Figure 9 shows the effectiveness of the ES voltage loop, where the predefined magnitude value of the ES voltage steps down from 120V to 60V. It's seen that the actual ES voltage can tracks the predefined value well, which can validate the analysis on the proposed decoupling mechanism.

When PCC voltage is used as reference vector, the power injected to PCC is directly related to i_{Gd} and i_{Gq}. Then, effective current loop is the key to realize the active power and reactive power independently. Two situations were selected for validation, as shown in Fig. 10.

In Fig. 10(a), i_{Gq} was kept to 0, i_{Gd} steps from 1.5A to 2.5A. In Fig. 10(b), i_{Gd} was kept at 2A while i_{Gq} steps from -1A to 1A. Meanwhile, the actual current $i_{G\alpha}$ and

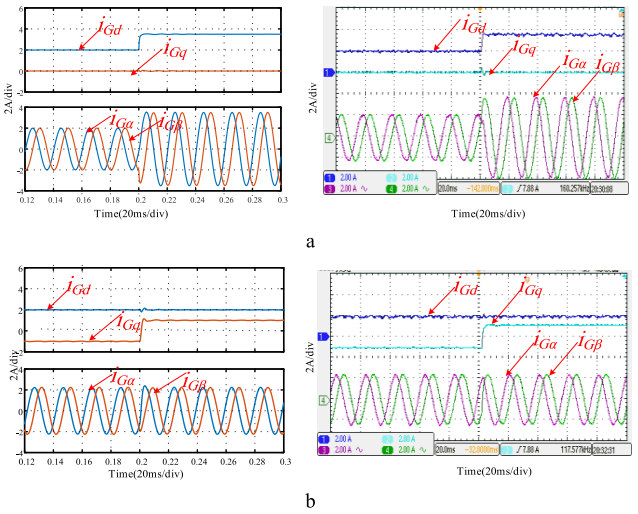

FIGURE 10. Simulation and experiment waveforms of current loop. a i_{Gd} step from 1A to 2.5A @ $i_{Gq} = 0$A b i_{Gq} step from −1A to 1A @ $i_{Gd} = 2$A.

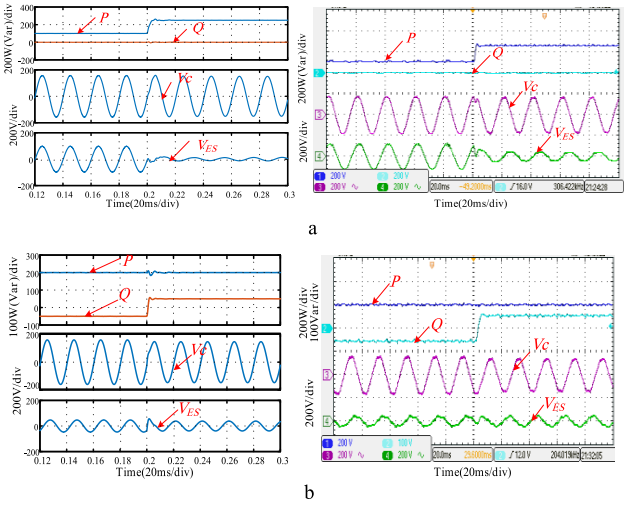

FIGURE 11. Simulation and experiment waveforms of power loop. a P step from 150W to 250W @ Q = 0Var b Q step from −50Var to 50Var @ P = 200W.

constructed virtual current $i_{G\beta}$ were also recorded. Simulation and experimental results are almost similar to each other, both of which validate the theoretical analysis.

Power loop is to make sure the injected power equal to the predefined value. Same as the current loop, two situations were provided, as shown in Fig. 11. In Fig. 11(a), Q was kept to 0 while P steps from 150W to 250W. In Fig. 11(b), P was 200W while Q steps from −50 to 50Var. Meanwhile, the PCC voltage and ES voltage were also recorded. It is also seen that the transient time is only several milliseconds.

From the results above, it's obviously seen that the proposed control achieves higher dynamic responses at power transients while the PCC voltage is kept stable, which has verified the proposed power decoupled control.

VI. CONCLUSION

In this paper, a new type of decoupled power control is proposed for ES-2 in the applications such households microgrids. Compared to existing power control for ES-2, system modeling with more analysis for parameters tuning and more functions are added. For instance, decoupling network is added as well as the inner current loop, which can achieve power decoupling and higher dynamic responses. Besides, more in-depth analysis including detailed system modeling and parameter tuning are provided. A simple discussion about the ability of active and reactive regulation of ES-2 is provided. In order to establish the mathematical model of ES-2 in dq axis synchronous rotating reference frame, SOGI algorithm and FAE were introduced to construct the virtual orthogonal voltage and current signals. Then, the detailed power decoupling control method was well illustrated. The PCC voltage was selected as the reference vector, helping decompose the injected current into active and reactive components, by controlling which the independent power control can be achieved only using PI controllers. Besides, an additional ES voltage loop was introduced to promise the premise tracking of the ES voltage. Finally, the effectiveness of the proposed decoupled power control is verified by both simulation and experimental results.

REFERENCES

[1] H. Hu, P. Pan, Y. Song, and Z. He, "A novel controlled frequency band impedance measurement approach for single-phase railway traction power system," *IEEE Trans. Ind. Electron.*, vol. 67, no. 1, pp. 244–253, Jan. 2020.
[2] L. Wang, C.-S. Lam, and M.-C. Wong, "Hybrid structure of static var compensator and hybrid active power filter (SVC//HAPF) for medium-voltage heavy loads compensation," *IEEE Trans. Ind. Electron.*, vol. 65, no. 6, pp. 4432–4442, Jun. 2018.
[3] Q. Xu, J. Xiao, X. Hu, P. Wang, and M. Y. Lee, "A decentralized power management strategy for hybrid energy storage system with autonomous bus voltage restoration and state-of-charge recovery," *IEEE Trans. Ind. Electron.*, vol. 64, no. 9, pp. 7098–7108, Sep. 2017.
[4] M. Shad, A. Momeni, R. Errouissi, C. P. Diduch, M. E. Kaye, and L. Chang, "Identification and estimation for electric water heaters in direct load control programs," *IEEE Trans. Smart Grid*, vol. 8, no. 2, pp. 947–955, Nov. 2017.
[5] T. Namerikawa, N. Okubo, R. Sato, Y. Okawa, and M. Ono, "Real-time pricing mechanism for electricity market with built-in incentive for participation," *IEEE Trans. Smart Grid*, vol. 6, no. 6, pp. 2714–2724, Nov. 2015.
[6] S. Y. Hui, C. K. Lee, and F. F. Wu, "Electric Springs—A new smart grid technology," *IEEE Trans. Smart Grid*, vol. 3, no. 3, pp. 1552–1561, Sep. 2012.
[7] S.-C. Tan, C. K. Lee, and S. Y. Hui, "General steady-state analysis and control principle of electric springs with active and reactive power compensations," *IEEE Trans. Power Electron.*, vol. 28, no. 8, pp. 3958–3969, Aug. 2013.
[8] S. Yan, C.-K. Lee, T. Yang, K.-T. Mok, S.-C. Tan, B. Chaudhuri, and S. Y. R. Hui, "Extending the operating range of electric spring using back-to-back converter: Hardware implementation and control," *IEEE Trans. Power Electron.*, vol. 32, no. 7, pp. 5171–5179, Jul. 2017.
[9] C. K. Lee and S. Y. R. Hui, "Input AC voltage control bi-directional power converters," U.S. Patent 13 907 350, May 31, 2013.
[10] N. R. Chaudhuri, C. K. Lee, B. Chaudhuri, and S. Y. R. Hui, "Dynamic modeling of electric springs," *IEEE Trans. Smart Grid*, vol. 5, no. 5, pp. 2450–2458, Sep. 2014.
[11] C. K. Lee and S. Y. R. Hui, "Reduction of energy storage requirements in future smart grid using electric springs," *IEEE Trans. Smart Grid*, vol. 4, no. 3, pp. 1282–1288, Sep. 2013.
[12] Q. Wang, M. Cheng, and Z. Chen, "Steady-state analysis of electric springs with a novel δ control," *IEEE Trans. Power Electron.*, vol. 30, no. 12, pp. 7159–7169, Dec. 2015.
[13] K.-T. Mok, S.-C. Tan, and S. Y. R. Hui, "Decoupled power angle and voltage control of electric springs," *IEEE Trans. Power Electron.*, vol. 31, no. 2, pp. 1216–1229, Feb. 2016.

[14] Y. Shuo, S.-C. Tan, C. K. Lee, and S. Y. R. Hui, "Electric spring for power quality improvement," in *Proc. IEEE Appl. Power Electron. Conf. Expo (APEC)*, Mar. 2014, pp. 2140–2147.
[15] C. K. Lee, N. R. Chaudhuri, B. Chaudhuri, and S. Y. R. Hui, "Droop control of distributed electric springs for stabilizing future power grid," *IEEE Trans. Smart Grid*, vol. 4, no. 3, pp. 1558–1566, Sep. 2013.
[16] M.-H. Wang, K.-T. Mok, S.-C. Tan, and S. Y. R. Hui, "Multifunctional DC electric springs for improving voltage quality of DC grids," *IEEE Trans. Smart Grid*, vol. 9, no. 3, pp. 1552–1561, May 2018.
[17] R. Zhang, M. Cardinal, P. Szczesny, and M. Dame, "A grid simulator with control of single-phase power converters in D-Q rotating frame," in *Proc. IEEE 33rd Annu. IEEE Power Electron. Spec. Conf.*, Jun. 2003, pp. 1431–1436.
[18] A. Roshan, R. Burgos, A. C. Baisden, F. Wang, and D. Boroyevich, "A D-Q frame controller for a full-bridge single phase inverter used in small distributed power generation systems," in *Proc. 27nd Annu. IEEE Appl. Power Electron. Conf. Expo. (APEC)*, Feb. 2007. pp. 641–647.
[19] C. Xie, K. Li, J. Zou, and J. M. Guerrero, "Passivity-based stabilization of LCL-type grid-connected inverters via a general admittance model," *IEEE Trans. Power Electron.*, to be published, doi: 10.1109/tpel.2019.2955861.
[20] R.-Y. Kim, S.-Y. Choi, and I.-Y. Suh, "Instantaneous control of average power for grid tie inverter using single phase D-Q rotating frame with all pass filter," in *Proc. 30th Annu. Conf. IEEE Ind. Electron. Soc.*, Busan, South Korea, May 2005, pp. 274–279.
[21] B. Bahrani, A. Rufer, and S. Kenzelmann, "Vector control of single- phase voltage-source converters based on fictive-axis emulation," *IEEE Trans. Ind Appl.*, vol. 47, no. 2, pp. 831–840, Dec. 2011.
[22] Q. Wang, M. Cheng, Y. Jiang, W. Zuo, and G. Buja, "A simple active and reactive power control for applications of single-phase electric springs," *IEEE Trans. Ind. Electron.*, vol. 65, no. 8, pp. 6291–6300, Aug. 2018.
[23] C. Bao, X. Ruan, X. Wang, W. Li, D. Pan, and K. Weng, "Step-by-step controller design for LCL-type grid-connected inverter with capacitor-current-feedback active-damping," *IEEE Trans. Power Electron.*, vol. 29, no. 3, pp. 1239–1253, Mar. 2014.
[24] D. Zmood and D. Holmes, "Stationary frame current regulation of PWM inverters with zero steady-state error," *IEEE Trans. Power Electron.*, vol. 18, no. 3, pp. 814–822, May 2003.
[25] F. Xiao, L. Dong, L. Li, and X. Liao, "A frequency-fixed SOGI-based PLL for single-phase grid-connected converters," *IEEE Trans. Power Electron.*, vol. 32, no. 3, pp. 1713–1719, Mar. 2017.

QINGSONG WANG (Senior Member, IEEE) received the B.Sc. and M.Sc. degrees from the Department of Electrical Engineering, Zhejiang University, Hangzhou, China, in 2004 and 2007, respectively, and the Ph.D. degree from the School of Electrical Engineering, Southeast University, Nanjing, China, in 2016. From November 2015 to November 2016, he was a Joint Ph.D. Student with the Department of Energy Technology, Aalborg University, Aalborg, Denmark, where he focused on electric springs.

From July 2004 to July 2005, he was an Engineer with Shihlin Electronic and Engineering Company, Ltd., Suzhou, China. From July 2007 to August 2011, he was an Engineer with the Global Development Center, Philips Lighting Electronics, Shanghai, China. In October 2010, he was promoted to be a Senior Engineer. From August 2011 to September 2013, he was a Lecturer with the PLA University of Science and Technology, Nanjing, China. Since 2017, he has been with Southeast University, where he is currently a Lecturer with the School of Electrical Engineering. He is also with the Jiangsu Key Laboratory of Smart Grid Technology and Equipment. His research interest is focused in the areas of control and applications of power electronics to power systems.

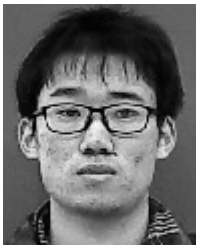

WUJIAN ZUO received the B.Sc. degree from Nanjing Tech University, Nanjing, China, in 2015, and the M.Eng. degree from the School of Electrical Engineering, Southeast University, Nanjing, in 2019.

He is currently with State Grid Huzhou Power Supply Company, Huzhou, China. His current research interest includes the applications of power electronics to power systems.

MING CHENG (Fellow, IEEE) received the B.Sc. and M.Sc. degrees from the Department of Electrical Engineering, Southeast University, Nanjing, China, in 1982 and 1987, respectively, and the Ph.D. degree from the Department of Electrical and Electronic Engineering, The University of Hong Kong, Hong Kong, in 2001.

Since 1987, he has been with Southeast University, where he is currently a Professor with the School of Electrical Engineering and the Director of the Research Center for Wind Power Generation. His teaching and research interests include electrical machines, motor drives for electric vehicles, and renewable energy generation. He has authored or coauthored more than 300 technical articles and four books and is the holder of 55 patents in these areas.

Prof. Cheng is a Fellow of the Institution of Engineering and Technology (IET). He has served as a Chair and an Organizing Committee Member for many international conferences. He is a Distinguished Lecturer of the IEEE Industry Applications Society (IAS), from 2015 to 2016.

FUJIN DENG (Member, IEEE) received the B.Eng. degree in electrical engineering from the China University of Mining and Technology, Jiangsu, China, in 2005, the M.Sc. degree in electrical engineering from Shanghai Jiao Tong University, Shanghai, China, in 2008, and the Ph.D. degree in energy technology from the Department of Energy Technology, Aalborg University, Aalborg, Denmark, in 2012. From 2013 to 2015 and from 2015 to 2017, he was a Postdoctoral Researcher and an Assistant Professor with the Department of Energy Technology, Aalborg University, Aalborg, Denmark. In 2017, he joined Southeast University, Nanjing, China, where he is currently a Professor with the School of Electrical Engineering. His main research interests include wind power generation, multilevel converters, high-voltage direct-current (HVDC) technology, DC grid, and offshore wind farm-power systems dynamics.

GIUSEPPE BUJA (Life Fellow, IEEE) received the Laurea degree (Hons.) in power electronics engineering from the University of Padova, Padua, Italy. He is currently a Full Professor with the University of Padova. He has carried out an extensive research work in the field of power and industrial electronics, originating the modulating-wave distortion and the optimum modulation for pulse-width modulation inverters, pioneering the introduction of digital signal processing in the control systems of power electronics converters, and conceiving advanced techniques for the control of electric drives. His current research interests are automotive electrification, including wireless charging of electric vehicles, and grid-integration of renewable energies.

Dr. Buja is a Senior Member of the Administrative Committee of the IES. He received the IEEE Industrial Electronics Society (IES) Eugene Mittelmann Achievement Award in recognition of his outstanding technical contributions to the field of industrial electronics, and the 2016 Best Paper Award from the IEEE TRANSACTIONS ON INDUSTRIAL ELECTRONICS. He has served the IEEE in several capacities, including as General Chairman of the 20th Annual Conference of the IES (IECON), in 1994. He is currently an Associate Editor of the IEEE TRANSACTIONS ON INDUSTRIAL ELECTRONICS and a member of the Editorial Board of the *Chinese Journal of Electrical Engineering*.